University of Bristol - Explore Bristol Research
General rights
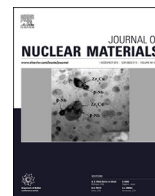
Structural effects in UO$_2$ thin films irradiated with fission-energy Xe ions

A.J. Popel [a], [*], V.A. Lebedev [b], P.G. Martin [c], A.A. Shiryaev [d], [b], G.I. Lampronti [a], R. Springell [c], S.N. Kalmykov [b], [e], T.B. Scott [c], I. Monnet [f], C. Grygiel [f], I. Farnan [a]

[a] Department of Earth Sciences, University of Cambridge, Downing Street, Cambridge, CB2 3EQ, United Kingdom
[b] Lomonosov Moscow State University, Moscow, 119991, Russia
[c] Interface Analysis Centre, School of Physics, University of Bristol, Bristol, BS8 1TL, United Kingdom
[d] Frumkin Institute of Physical Chemistry and Electrochemistry RAS, Moscow, Russia
[e] National Research Centre "Kurchatov Institute", 123098, Moscow, Russia
[f] CIMAP, CEA-CNRS-ENSICAEN-Université de Caen, BP 5133, 14070, Caen, Cedex5, France

HIGHLIGHTS

- Flat (001) single crystal UO$_2$ thin films on LSAT (001) substrates produced.
- Ion irradiation induced topographical and structural rearrangements in UO$_2$ films.

ARTICLE INFO

ABSTRACT

Uranium dioxide thin films have been successfully grown on LSAT (Al$_{10}$La$_3$O$_{51}$Sr$_{14}$Ta$_7$) substrates by reactive magnetron sputtering. Irradiation by 92 MeV ^{129}Xe^{23+} ions to simulate fission damage that occurs within nuclear fuels caused microstructural and crystallographic changes. Initially flat and continuous thin films were produced by magnetron sputtering with a root mean square roughness of 0.35 nm determined by AFM. After irradiation, this roughness increased to 60–70 nm, with the films developing discrete microstructural features: small grains (~3 μm), along with larger circular (up to 40 μm) and linear formations with non-uniform composition according to the SEM, AFM and EDX results. The irradiation caused significant restructuring of the UO$_2$ films that was manifested in significant film-substrate mixing, observed through EDX analysis. Diffusion of Al from the substrate into the film in unirradiated samples was also observed.

© 2016 The Authors. Published by Elsevier B.V. This is an open access article under the CC BY license (http://creativecommons.org/licenses/by/4.0/).

1. Introduction

Uranium dioxide, UO$_2$, is the form of nuclear fuel used in the present generation of most nuclear reactors [1–4]. The knowledge and understanding of its in-reactor behaviour and its stability under subsequent storage and disposal conditions are of great technological importance [1,5].

The heat generated within nuclear fuels comes from the slowing down of fission fragments produced by fission events [6]. These fission products possess large kinetic energies (in the range 70–100 MeV) with high linear energy transfer, dE/dx, of 18–22 keV/

nm for light and heavy fission fragments, respectively [7,8]. As a result, heat and radiation damage are produced inside fuel pellets, leading to the degradation of the fuel's properties [6,7,9,10].

The current work considers the effects of radiation damage by swift heavy ions on the structural stability of the UO$_2$ matrix. Although this topic has received and continues to receive a lot of attention [4–6,10–18], the emphasis of the current work is on the impact of ions with the mass and energy characteristics of fission fragments [7] onto thin films of UO$_2$. These samples can be readily analysed with a wide range of analytical techniques and compared with actual spent fuel.

For this purpose, thin films of uranium dioxide were deposited on LSAT (Lanthanum Strontium Aluminium Tantalum oxide) substrates and irradiated with 92 MeV ^{129}Xe^{23+} ions to a fluence of 4.8 × 10^{15} ions/cm^2. The irradiated and as-produced films were

analysed for comparison using XRD (X-ray Diffraction), GISAXS (Grazing Incidence Small Angle X-ray Scattering), SEM (Scanning Electron Microscopy), EDX (Energy Dispersive X-ray spectroscopy), AFM (Atomic Force Microscopy), EBSD (Electron Backscatter Diffraction) and XPS (X-ray Photoelectron Spectroscopy) techniques. The results obtained from the XPS study are presented in Ref. [19].

2. Experimental details

2.1. Sample production

Thin films of uranium dioxide were produced by reactive sputtering onto single crystal LSAT substrates with (001), (110) and (111) orientations using a similar methodology to that outlined previously for LaAlO₃, CaF₂ [20] and YSZ (Yttrium Stabilised Zirconia) substrates [25]. Table 1 summarises the samples produced.

A dedicated DC magnetron sputtering facility with UHV base pressure (10^{-9} mbar) was employed for the growth of films at the University of Bristol. A depleted uranium metal target was used as a source of uranium and the magnetron gun was kept at a power of 50 W by controlled direct current of 0.11–0.14 A and the corresponding voltage of 350–450 V, giving a growth rate of 0.9–1.1 Å/s. Argon was used as the sputtering gas at a pAr in the range of $7-8 \times 10^{-3}$ mbar. Oxygen was used as the reactive gas at a pO₂ in the range $3.4-4.4 \times 10^{-5}$ mbar. Throughout film growth the LSAT substrates were maintained at a temperature close to 750 °C.

The substrates were single crystal LSAT polished on one side with dimensions of $10 \times 10 \times 0.5$ mm supplied by MTI Corp, USA. LSAT has a cubic perovskite structure with $a_{LSAT} = 3.868$ Å [21] and UO₂ has a cubic fluorite structure with $a_{uo_2} = 5.469$ Å, both at room temperature [20]. This results in the epitaxial relationship in which the (001) plane of UO₂ is rotated by 45° in relation to the (001) plane of LSAT so that the (110) plane of UO₂, with a d-spacing $a_{uo_2}/\sqrt{2} = 3.867$ Å, fits the LSAT (001) plane, with a d-spacing of 3.868 Å ($= a_{LSAT}$), as was described by Bao et al. [20] for a UO₂ film on a LaAlO₃ substrate. This mismatch causes the UO₂ lattice to be only at a slight tension of +0.03% with respect to the substrate in-plane spacing. This 45° rotation epitaxial relationship only holds between the LSAT and UO₂ (001) planes.

Post fabrication, the thin films (and substrates) were cut into two halves using a diamond saw, such that one half could be used for ion irradiation, whilst the other half was left as a control for comparison measurements. The irradiated halves are denoted by an asterisk,*, in the sample numbering scheme.

2.2. Sample irradiation

To simulate the damage produced by fission fragments in nuclear fuel, the samples were irradiated with 92 MeV energy ^{129}Xe^{23+} ions to a fluence of 4.8×10^{15} ions/cm² on the IRRSUD beamline at the GANIL accelerator, Caen, France. The beamline base vacuum was 6×10^{-7} mbar during the irradiation. The flux was

kept at ca. 1.3×10^{10} ions/(cm² s) which caused heating of the samples to a temperature not exceeding 150 °C. The temporal structure of the ion beam was 1 ns ion pulse every 100 ns and the beam was swept across the surface of the samples with a frequency of 400 Hz in the horizontal and 4 Hz in the vertical direction to ensure homogenous irradiation. The samples were allowed to cool down to ambient temperature (~19 °C) before the beamline was brought to atmospheric pressure using nitrogen gas to minimise surface oxidation of the samples.

According to the SRIM-2013.00 software [22], the expected nuclear and electronic stopping, dE/dx, for 92 MeV Xe ions in UO₂ is 0.26 and 24.6 keV/nm, respectively, and the projected ion range is ~6.5 μm. A theoretical UO₂ density of 10.96 g/cm³ [8] was assumed in the SRIM calculation. The SRIM results indicate that the Xe ions completely penetrate the UO₂ thin films (140 nm max) and the electronic stopping regime dominates the dissipation of ion energy throughout the entire film. The Xe ions stop in the substrate at a depth of ~7.3 μm beneath the sample's surface.

2.3. Sample characterisation

To assess the crystallographic orientations of the produced films and structural rearrangements caused by the ion irradiation, XRD and EBSD techniques were applied.

The samples were analysed in Bragg-Brentano geometry on a D8 Bruker X-ray diffractometer equipped with a primary Ge monochromator for Cu Kα1 and a Sol-X solid state detector. The irradiated samples were also investigated in Bragg-Brentano geometry on an Empyrean (Panalytical) diffractometer with a Ni-filter and X'Celerator detector and on a Rigaku D/MAX 2500 diffractometer with rotating copper anode and curved graphite [002] monochromator for Cu Kα1,2 installed on the secondary beam. Samples were spun during signal collection in all cases. The results obtained on these different machines are complementary due to accessibility of different regions of reciprocal space. In addition, the samples were also studied in Grazing Incidence geometry (GIXRD) with incident angles between 0.5 and 2.5°.

Grazing incidence small-angle X-ray scattering patterns were obtained using a dedicated setup on a SAXSess (Anton Paar). The patterns were recorded at several incident angles between 0.005 and 0.2°. Note, however, that the accuracy of the stage orientation is ±0.005° and in some cases images reflect relative differences rather than the absolute angular values.

EBSD instrumentation from AMETEK-EDAX associated with a Zeiss SIGMA™ Variable Pressure SEM fitted with a Gemini™ field emission electron column and Digiview 3 high speed camera were used. The diffraction data acquired from EBSD analysis were recorded and processed using OIM™ software, which produced crystallographic orientation and phase maps from predefined surface areas using an automated mapping routine. A conductive bridge was formed with a silver paste between the surface of the samples and the sample stage to mitigate surface charging.

The surface morphology of the films was examined by means of SEM and AFM. AFM images were obtained on NT-MDT N'Tegra Aura atomic force microscope with the use of diamond ART-300 tips (Artech Carbon) with a radius of <10 nm and cantilever resonance frequency of approximately 300 kHz. XYZ tip movements were performed by pre-calibrated closed-loop piezotube scanner with capacity sensors. Errors, caused by scanner geometry and non-linearities, were less than 3% for XY-directions and 5% − for the Z direction. Images were measured in the repulsive regime of tapping-mode. Free amplitude of the tip oscillations was in the range 100–200 nm for flat surfaces and up to 500 nm in the cases of highly damaged surfaces. The oscillation amplitude value of 60–75% of the free amplitude was used as a feedback signal for the

Table 1
Summary of the crystallographic indices (hkl) for the substrates and UO₂ films and thicknesses of the UO₂ films measured using transverse SEM on a cross section of each sample.

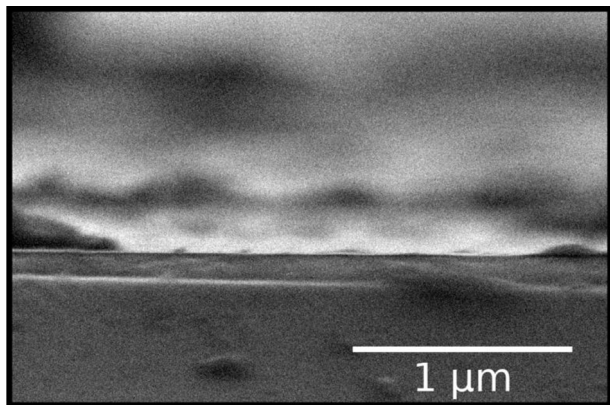| Sample name	(hkl)		Film thickness (nm) (±10%)
	LSAT substrate	UO₂ film	
SN489	(111)	(210)[a]	110
SN490	(001)	(001)	140
SN491	(001)	(001)	120
SN492	(110)	(111)[a]	140

[a] Preferential crystallographic orientation.

Fig. 1. A secondary electron SEM image of the cross section of sample SN489. The top of the substrate is delineated by the white line about 1/3 from the bottom of the image.

surface topography tracking. The Lateral probe movement rate was lower than 10 μm/min.

SEM images were obtained using a Zeiss Leo Supra 50VP scanning electron microscope equipped with an X-Max 80 mm^2 EDX detector (Oxford Instruments). To reduce the charging effects on the sample, the analysis was performed in a low-vacuum regime, with a 39 Pa pressure of nitrogen and a variable pressure secondary electron (VPSE) detector used to acquire images.

Thickness of the films was measured using SEM at the cut cross sections. All SEM and AFM images were processed with the open-source software Gwyddion [23]. Surface composition was examined using EDX. The EDX spectral deconvolution and elemental quantification were performed using the INCA software (Oxford Instruments) with ZAF-correction. Before every series of EDX measurements, signal intensity was recalibrated in low-vacuum mode using a Co standard sample.

3. Results

3.1. Film thickness

Film thickness is one of the key parameters for thin films and was measured using transverse SEM on a cross section of the sample (Fig. 1). Table 1 summarises the measured thicknesses, which ranged from 110 to 140 nm.
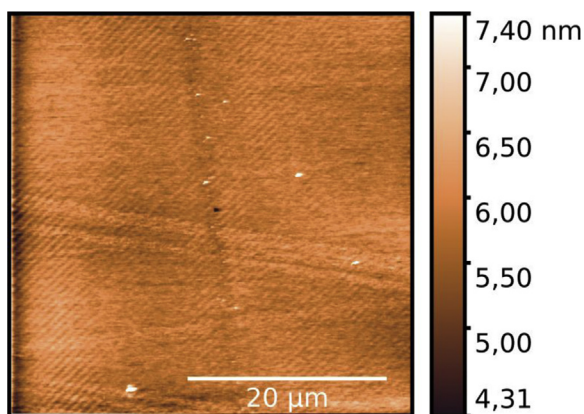

Fig. 2. An AFM image of the surface topography of sample SN492. The regular fluctuations are attributed to instrumental effects for a very flat surface. (For interpretation of the references to colour in this figure legend, the reader is referred to the web version of this article.)
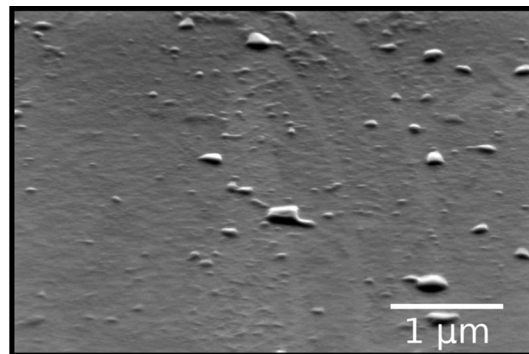

Fig. 3. A secondary electron SEM image of the surface topography of sample SN490 showing presence of contaminants.

3.2. Surface topography

The unirradiated samples all show similar surface topography in both SEM and AFM studies. Samples are generally flat and AFM measurements (Fig. 2) give the root mean square (RMS) roughness as low as 0.35 nm, which lies close to the instrumental limit, and average height variation of 5.8 nm over the area of 40×40 μm for a contamination-free region of the sample. Particulate contamination was observed on the surface of the samples and can be seen in Fig. 3. These contaminant particles are densely populated and have dimensions down to 30 nm, and likely to persist throughout the entire film volume.

A contaminant film was observed on the uranium dioxide surface during the SEM, AFM and GISAXS studies. The results of EDX and XPS [19] studies indicated that this film is carbonaceous in nature. AFM imaging of the surfaces was complicated by the cantilever having to penetrate through this contaminant film in order to reach the UO_2 surface below. Also, the mechanical properties of the film have a strong influence on the cantilever's tip movements and, therefore, on the quality of AFM images. As a result, AFM images of the UO_2 film were produced only for samples SN491 and SN492. The GISAXS results obtained at shallow incidence angle (nominally 0.005°, not shown) support the presence of the carbonaceous film by showing the specular reflection with some contribution from disordered material that disappears at steeper angles of incidence.
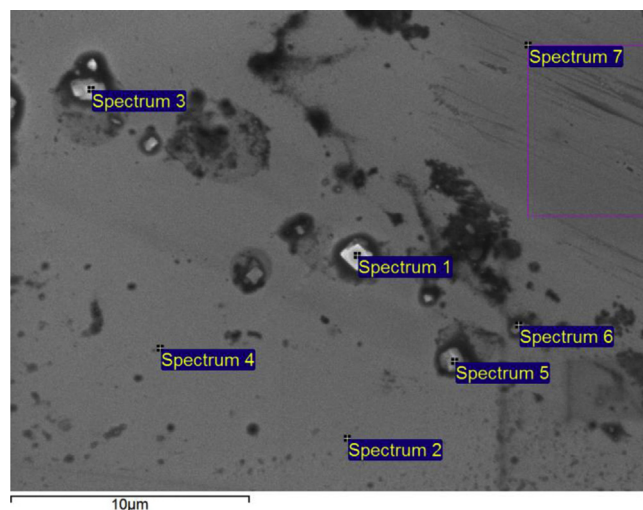

Fig. 4. A secondary electron SEM image showing the EDX elemental analysis points on the surface of sample SN489, with the quantification results shown in Table 2.

Table 2
Summary of the EDX results for sample SN489 at the points shown in Fig. 4 (accelerating voltage 10 kV).

at%	C	O	Al	Cl	Nb	U
Spectrum 1	56	14	bdl[a]	18	1.2	11
Spectrum 2	67	24	bdl	bdl	1.1	8
Spectrum 3	63	14	bdl	15	0.7	7
Spectrum 4	64	26	bdl	bdl	1.2	9
Spectrum 5	53	22	bdl	11	1.4	13
Spectrum 6	57	24	0.7	1	1.9	15
Spectrum 7	33	49	0.9	bdl	1.9	16

[a] bdl – below detection limit.

Contamination assessment with EDX indicated carbon (~60 at%) and niobium (~1–2 at%) present in the films. Chlorine containing particles were observed on the surface of sample SN489 (Fig. 4 and Table 2). Trace amounts of aluminium (~0.8 at%) were also observed in the films. The XPS study [19] confirmed the presence of carbon and niobium contamination and indicated that Nb is present in the Nb^{5+} oxidation state. Hence, it is likely that niobium is present as Nb_2O_5 and located mainly in the particulate contaminants distributed throughout the UO_2 films.

The ion irradiation caused significant restructuring of the films (Fig. 5). A discrete circular (hillock-like) microstructure was formed, with typical features for sample SN489* being 1–6 μm, SN491* (SN490* behaved identically to SN491*) 2–10 μm and for SN492* 0.5–5 μm. This circular microstructure produced in sample SN492* exhibits a more regular shape and is smaller in size when compared to other samples. All samples exhibit greater circular features. Note that these features were visible in a conventional light microscope.

Lower magnification SEM images (Fig. 6) show that the UO_2 films on the substrates with different crystallographic orientations exhibit different microstructural patterns at the surface after the ion irradiation. Samples SN490* and SN491* (both with UO_2 in (001), originally) exhibit densely populated regular lines intersecting at right angles. Sample SN492* (mostly (111) UO_2, originally) possesses fewer of these lines intersecting at different angles. For sample SN489* (preferentially (210) UO_2, originally) these lines were not observed at all. This difference and the origin of the lines are difficult to explain without the irradiated blank substrates.
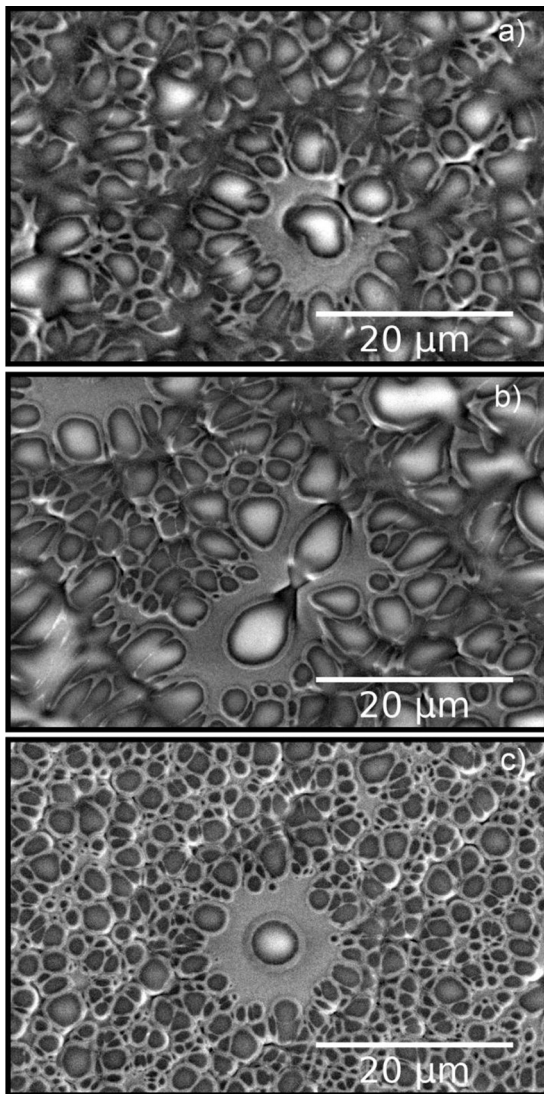

Fig. 5. Secondary electron SEM images of irradiated samples: a) SN489* (preferentially (210) UO_2, originally), b) SN491* (UO_2 in (001), originally), c) SN492* (mostly (111) UO_2, originally).
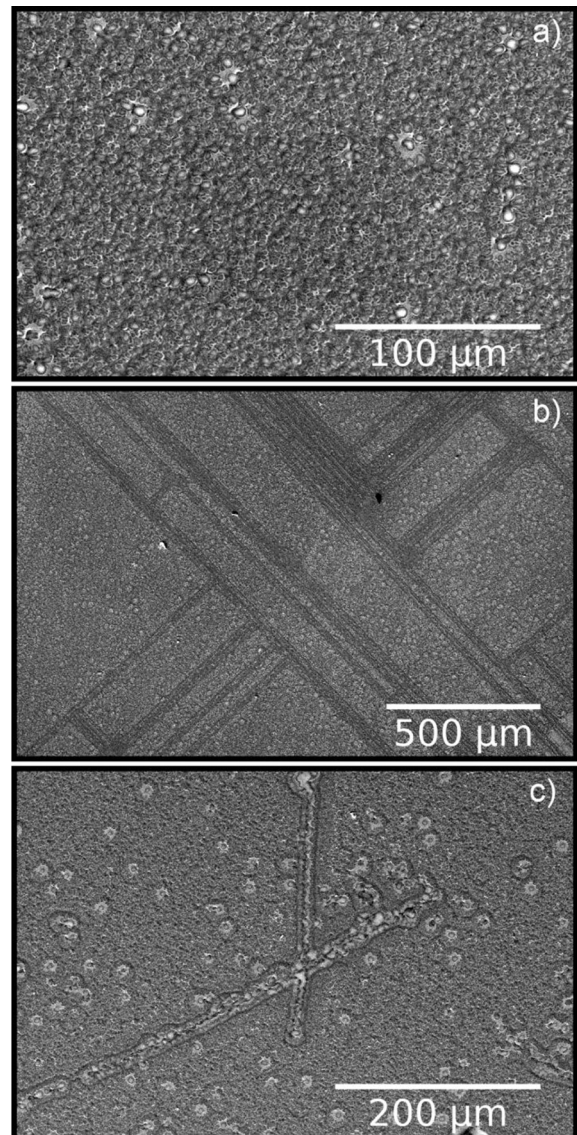

Fig. 6. Low magnification secondary electron SEM images of irradiated samples: a) SN489*, b) SN491*, c) SN492*.
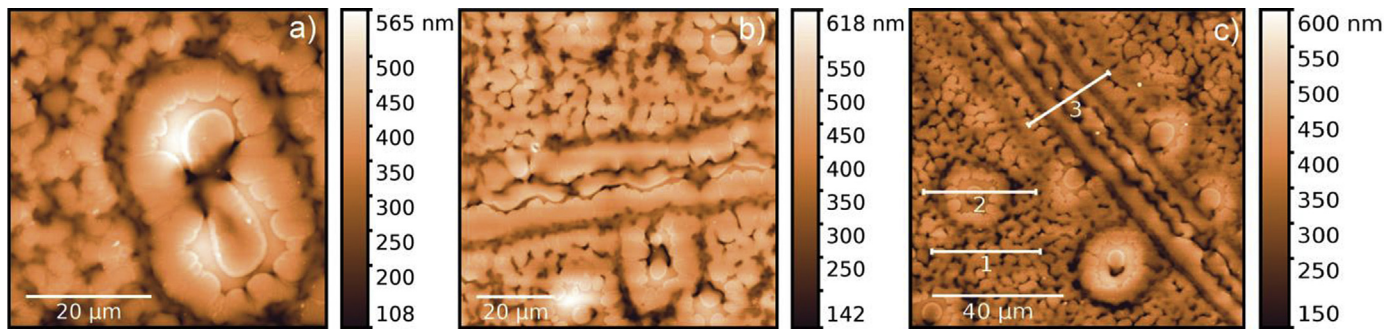
Fig. 7. AFM images of irradiated samples: a) SN489*, b) SN490*, c) SN492*. (For interpretation of the references to colour in this figure legend, the reader is referred to the web version of this article.)

Substrates restructuring might have affected the microstructure of the uranium dioxide films.

The surface profiles from the AFM study (Fig. 7) indicated formation of a characteristic "cauliflower" microstructure. In addition to forming discrete small grains (~3 μm), larger circular (up to 40 μm) and linear formations were observed. The RMS roughness increased to 60—70 nm and average height variation to 320—400 nm for the measurements over the area of 50 × 50 μm for sample SN489*, 80 × 80 μm for sample SN490* and 100 × 100 μm for sample SN492*. The cross-section profiles across the lines marked in Fig. 7c are shown in Fig. 8. The results obtained from the AFM study are consistent with the SEM results.
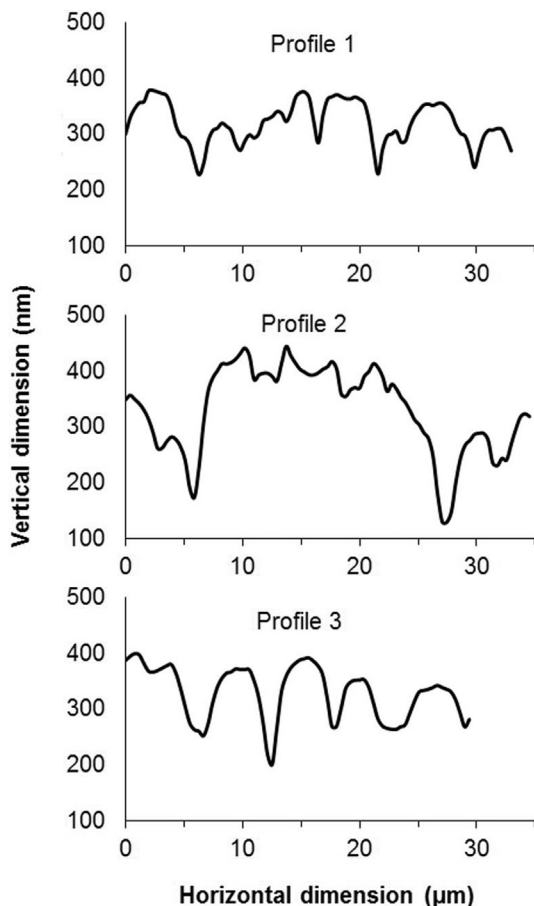
Results from the EDX analysis show that the arising microstructure is not uniform in elemental composition (Fig. 9 and Table 3). Hence, significant substrate-film mixing is indicated as a result of the ion irradiations, which is supported by the XPS study [19]. In the grey regions around the grains (for example, spectra 2, 5, 8) calculated uranium content is about twice that in the central regions of the grains (for example, spectra 1, 6, 7), with niobium and carbon contamination still persisting. The uranium content for irradiated sample SN492* (mostly (111) UO_2, originally) is about twice of that of irradiated sample SN490* (UO_2 in (001), originally), at the corresponding points of analysis. This suggests that the UO_2 film of sample SN492 is more resistant to mixing with the LSAT substrate than the film of sample SN490 as a result of the ion irradiation.

3.3. Crystallographic analysis

Results of the XRD studies for the samples show reflections for LSAT substrates and UO_2 films. In our experimental geometry, sample SN489 had only one peak at $2\theta = 77.9°$ which can be identified as 420 reflection of UO_2 (see Fig. 10). Samples SN490 and SN491 showed 200, 400 and 600 UO_2 reflections. Sample SN492 showed strong 111, 222 and 333 and much weaker 220 and 311 UO_2 reflections.

Only for samples SN490 and SN491 was it possible to obtain EBSD maps of the samples' surface. The inverse pole figure (IPF) crystallographic orientation map for samples SN490 and SN491 (Fig. 11) indicated that the surface of these samples has (001) crystallographic orientation. The diffraction signal from samples SN489 and SN492 was too weak to construct a diffraction map of the surface, most likely, due to carbonaceous film deposit on the surface of the UO_2 film. For sample SN489 the diffraction pattern was identical from different points at the surface of the sample, which implies the same crystallographic orientation between the points, which is characteristic of single crystal samples. For sample SN492 considerable heterogeneity was observed in the diffraction pattern at different points studied, which implies different crystallographic orientations between the points. It is characteristic for polycrystalline materials.

Based on the expected epitaxial relationship for a UO_2 film on the LSAT (001) substrate and the obtained results from the XRD and EBSD studies, we suggest that the UO_2 films in samples SN490 and SN491 can be considered as single crystals, although further work is needed to prove this (for example, XRD in-plane φ scans as was described in the work by Strehle et al. [24]). Sample SN489 can be described as a preferentially oriented in (210) and sample SN492, most likely, is polycrystalline with a (111) preferred orientation.

Fig. 12a shows the 2D GISAXS pattern from unirradiated sample SN490 that has a clear anisotropic scattering due to crystallographically ordered material, confirming its single crystal nature.
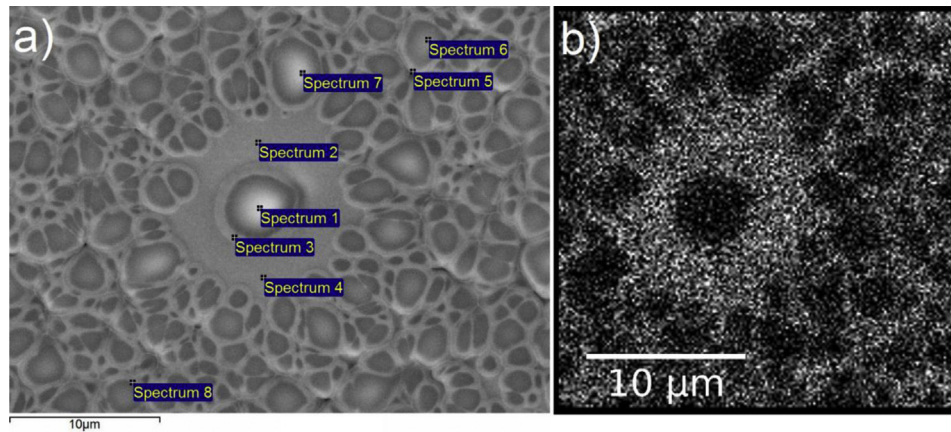

Fig. 8. Cross-section profiles across the lines marked in Fig. 7c.

Fig. 9. a) A secondary electron SEM image showing the EDX elemental analysis points, with the quantification results shown in Table 3, and b) EDX map of the U Mα1-line signal on the surface of irradiated sample SN492*.

From the XRD data for the irradiated samples it becomes evident that the ion irradiation resulted in noticeable structural rearrangements.

The diffraction pattern from sample SN489* (Fig. 10) showed that the UO_2 420 reflection disappeared and new ones appeared: UO_2 111, 311 and possibly 200 and 220. Uranium dioxide reflections 200 and 220 overlap with LSAT reflections 220 and 400, respectively. Reflection 111 from the substrate disappeared but 222, 333, 444 and 555 reflections persisted. An amorphous hump between 20 and 37° was also formed, ascribed to partial amorphisation of the substrate. The amorphisation is confirmed by the GISAXS results. The GISAXS pattern from irradiated sample SN490* (Fig. 12b) indicated amorphisation of the sample that follows from disappearance of the anisotropic scattering, weakening and blurring of the specular reflection.

Samples SN490* and SN491* retained the 200 and 400 UO_2 reflections. In addition to that, 111 and 311 UO_2 reflections appeared. Reflection 200 from the substrate disappeared but 400 persisted. An unidentified reflection at ~42° and an amorphous hump between 21.5 and 36° were also observed.

Sample SN492* retained the UO_2 reflections 111, 220 and 311. The UO_2 reflection 222 disappeared. Reflections from the substrate persisted. An amorphous hump between 20.5 and 33.5° was also observed.

Grazing incidence XRD measurements conducted over the irradiated samples show a poor diffraction pattern which indicates that the irradiated films were severely damaged. The exception is sample SN492* which still shows a well-defined diffraction pattern from the film (Fig. 13) that is consistent with the bulk XRD result.

No diffraction pattern was observed in the EBSD study from the irradiated samples. This was attributed to the considerable surface roughness caused by the ion irradiation.

Table 3
Summary of the EDX results for the irradiated sample SN492* at the points shown in Fig. 9a (accelerating voltage 20 kV).

at%	C	O	Al	Sr	Nb	La	Ta	U
Spectrum 1	25	47	8	9	0.4	4	4	2
Spectrum 2	44	38	4	3	0.8	2	2	6
Spectrum 3	35	43	5	5	0.8	2	2	6
Spectrum 4	44	38	4	3	0.9	2	2	6
Spectrum 5	28	47	6	5	0.8	3	3	8
Spectrum 6	31	45	7	7	0.4	3	3	3
Spectrum 7	27	46	7	8	0.5	4	4	3
Spectrum 8	32	44	6	6	0.7	3	3	5

4. Discussion

Uranium dioxide films can be grown successfully on LSAT with (001) and preferential (111) and (210) crystallographic orientations, as confirmed by the XRD and EBSD studies, and analysed with a range of analytical techniques.

A contamination layer on the film surfaces, most likely, is originating from the adsorption of atmospheric CO_2 and oil vapour from vacuum pumps used in the SEM, EBSD and XPS instruments.

Particulate contamination more likely comes from the deposits on the walls in the film growing chamber.

Aluminium incorporation into UO_2 films was also observed by Strehle et al. [24], when uranium dioxide films on sapphire (Al_2O_3) substrates were produced. It seems to be the case that aluminium containing substrates tend to give rise to Al incorporation into uranium dioxide films.

The microstructure resulted from the ion irradiation also went through some crystallographic rearrangements as evidenced by disappearance of some originally present and appearance of new UO_2 XRD reflections. We are inclined to suggest that in our case local overheating and recrystallization of the films took place as a result of the pulsed nature of the beam.

Disappearance of reflections from the low index planes of the substrates and persistence of reflections from the high index planes after the ion irradiation can be rationalised in terms of greater damage occurring to the top layer of the substrates which is responsible for the low index reflections. The low index reflections
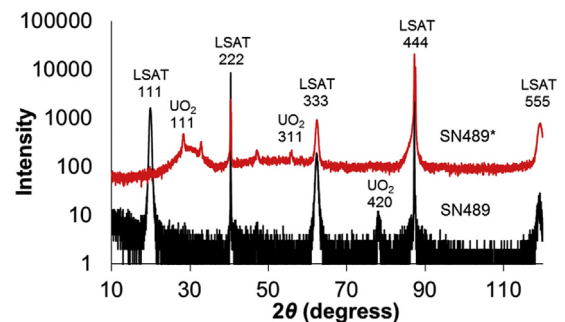

Fig. 10. XRD results for sample SN489 (bottom): unirradiated UO_2 film on LSAT (111) substrate analysed on a D8 Bruker diffractometer and sample SN489* (top): irradiated UO_2 film on LSAT (111) substrate analysed on a Rigaku D/MAX 2500 diffractometer. The peaks at ~33 and 47° can correspond to 200 and 220 reflections from the UO_2 film or 220 and 400 reflections from the LSAT substrate.
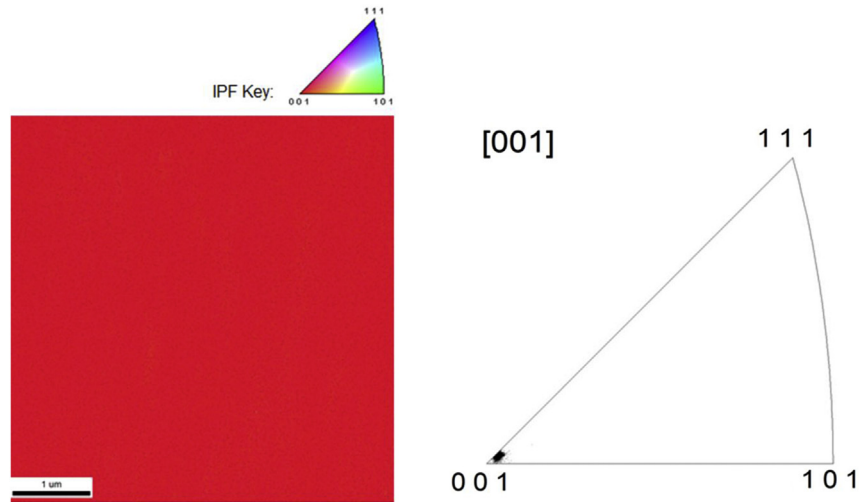
Fig. 11. EBSD results for sample SN491: the inverse pole figure map (left) and the corresponding inverse pole figure triangular diagram [19] (right). (For interpretation of the references to colour in this figure legend, the reader is referred to the web version of this article.)
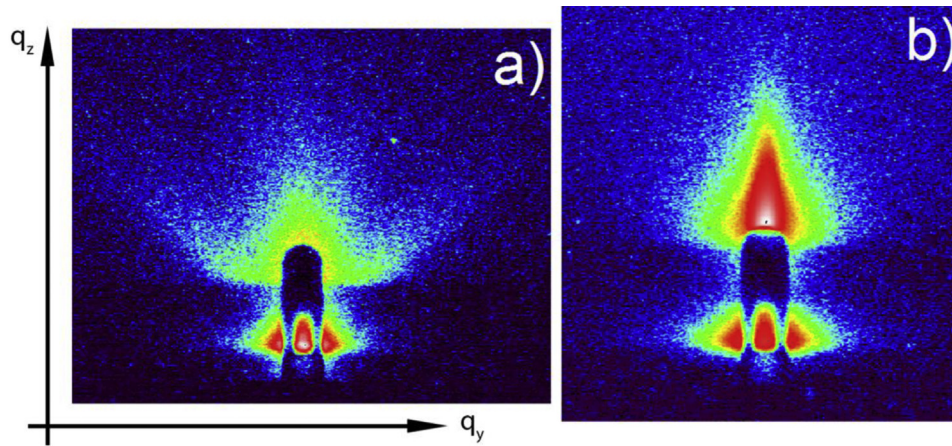

Fig. 12. 2D GISAXS pattern recorded at an incident angle 0.05° from: a) unirradiated sample SN490, b) irradiated sample SN490*. Red colour − high intensity, blue colour − low intensity. (For the colour version of this figure, the reader is referred to the web version of this article.)

correspond to lower values of 2θ, implying lower penetration depth of X-rays and higher sensitivity to the surface layer.

Since the xenon ions have a penetration depth of about 6.5 μm in UO_2 and the uranium dioxide films have a maximum thickness of 140 nm, the LSAT substrates were also subjected to irradiation damage. Unfortunately, no substrates without a UO_2 film were irradiated to assess crystallographic rearrangements in the single crystal LSAT substrates. In addition, some reflections from LSAT and UO_2 do overlap in XRD analysis. Hence, it is not possible to distinguish between some possible LSAT and UO_2 reflections that can result from the ion irradiation.

The mechanism for such a complex microstructural and crystallographic rearrangement due to the ion irradiation is not clear and requires further work. Blank substrates should be irradiated and characterised, along with thicker films. Irradiations with lower fluences should be performed. This will allow elucidating the onset of non-epitaxial recrystallization of the UO_2 matrix. Cross-sectional studies, including TEM-EDX (Transmission Electron Microscopy with EDX), SIMS (Secondary Ion Mass Spectrometry) and APT (Atomic Probe Tomography), would greatly assist in understanding the film-substrate mixing.

5. Conclusions

Single crystal LSAT substrates with (001) plane orientation are suitable for growing single crystal uranium dioxide films with the expected low strains. However, the detection of some aluminium migration into the films in this work would indicate that aluminium containing substrates might be not suitable in general
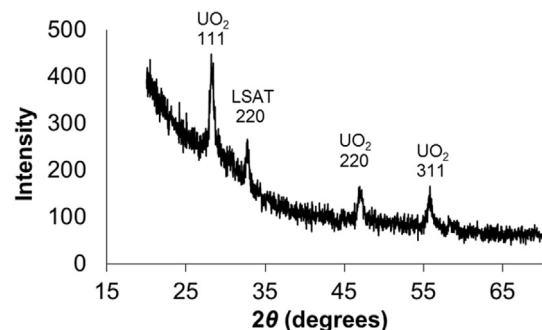

Fig. 13. GIXRD result for sample SN492*. Incident angle = 2.5°.

for production of high purity UO$_2$ films.

It has been shown that by irradiating thin films of UO$_2$ with high energy, high fluence ions it is possible to conduct studies on the response of the UO$_2$ matrix to radiation damage utilising advantages that thin films can offer: namely, ability to produce single crystal UO$_2$, as was shown in the work by Strehle et al. [24], to deal with a simplified idealised system and low amount of radioactive material that greatly simplifies handling of the samples.

Further work is required to understand the mechanism that is responsible for formation of the complex microstructure that resulted from the ion irradiation, including the observed crystallographic rearrangements.

Acknowledgments

Appendix A. Supplementary data

Supporting data will be available in A.J. Popel's PhD thesis (University of Cambridge) published online.

References

[1] H. He, Z. Qin, D.W. Shoesmith, Electrochim. Acta 56 (2010) 53–60.
[2] F. Garrido, L. Vincent, L. Nowicki, G. Sattonnay, L. Thomé, Nucl. Instr. Meth. Phys. Res. B 266 (2008) 2842–2847.
[3] F. Garrido, C. Choffel, J.-C. Dran, L. Thomé, L. Nowicki, A. Turos, Nucl. Instr. Meth. Phys. Res. B 127/128 (1997) 634–638.
[4] H.J. Matzke, A. Turos, G. Linker, Nucl. Instr. Meth. Phys. Res. B 91 (1994) 294–300.
[5] H.J. Matzke, J. Nucl. Mater 190 (1992) 101–106.
[6] H.J. Matzke, Nucl. Instr. Meth. Phys. Res. B 65 (1992) 30–39.
[7] H.J. Matzke, P.G. Lucuta, T. Wiss, Nucl. Instr. Meth. Phys. Res. B 166–167 (2000) 920–926.
[8] T. Wiss, H.J. Matzke, C. Trautmann, M. Toulemonde, S. Klaumünzer, Nucl. Instr Meth Phys. Res. B 122 (1997) 583–588.
[9] P.B. Weisensee, J.P. Feser, D.G. Cahill, J. Nucl. Mater 443 (2013) 212–217.
[10] N. Ishikawa, Y. Chimi, O. Michikami, Y. Ohta, K. Ohhara, M. Lang, R. Neumann, Nucl. Instr Meth Phys. Res. B 266 (2008) 3033–3036.
[11] L.F. He, J. Pakarinen, M.A. Kirk, J. Gan, A.T. Nelson, X.M. Bai, A. El-Azab, T.R. Allen, Nucl. Instr Meth Phys. Res. B 330 (2014) 55–60.
[12] V.G. Baranov, A.V. Lunev, V.F. Reutov, A.V. Tenishev, M.G. Isaenkova, A.V. Khlunov, J. Nucl. Mater 452 (2014) 147–157.
[13] T. Sonoda, M. Kinoshita, N. Ishikawa, M. Sataka, A. Iwase, K. Yasunaga, Nucl. Instr Meth Phys. Res. B 268 (2010) 3277–3281.
[14] M. Kinoshita, K. Yasunaga, T. Sonoda, A. Iwase, N. Ishikawa, M. Sataka, K. Yasuda, S. Matsumura, H.Y. Geng, T. Ichinomiya, Y. Chen, Y. Kaneta, M. Iwasawa, T. Ohnuma, Y. Nishiura, J. Nakamura, H.J. Matzke, Nucl. Instr Meth Phys. Res. B 267 (2009) 960–963.
[15] A. Iwase, H. Ohno, N. Ishikawa, Y. Baba, N. Hirao, T. Sonoda, M. Kinoshita, Nucl. Instr Meth Phys. Res. B 267 (2009) 969–972.
[16] H. Ohno, A. Iwase, D. Matsumura, Y. Nishihata, J. Mizuki, N. Ishikawa, Y. Baba, N. Hirao, T. Sonoda, M. Kinoshita, Nucl. Instr Meth Phys. Res. B 266 (2008) 3013–3017.
[17] T. Sonoda, M. Kinoshita, Y. Chimi, N. Ishikawa, M. Sataka, A. Iwase, Nucl. Instr Meth Phys. Res. B 250 (2006) 254–258.
[18] H.J. Matzke, J. Spino, J. Nucl. Mater 248 (1997) 170–179.
[19] Y.A. Teterin, A.J. Popel, K.I. Maslakov, A.Y. Teterin, K.E. Ivanov, S.N. Kalmykov, R. Springell, T.B. Scott, I. Farnan, Inorg. Chem. 55 (2016) 8059–8070.
[20] Z. Bao, R. Springell, H.C. Walker, H. Leiste, K. Kuebel, R. Prang, G. Nisbet, S. Langridge, R.C.C. Ward, T. Gouder, R. Caciuffo, G.H. Lander, Phys. Rev. B 88 (2013) 134426.
[21] B.C. Chakoumakos, D.G. Schlom, M. Urbanik, J. Luine, J. Appl. Phys. 83 (1998) 1979–1982.
[22] J.F. Ziegler, J.P. Biersack, M.D. Ziegler, The Stopping and Range of Ions in Matter, SRIM Co., Chester, Maryland, U.S.A., 2008.
[23] D. Nečas, P. Klapetek, Cent. Eur. J. Phys. 10 (2012) 181–188.
[24] M.M. Strehle, B.J. Heuser, M.S. Elbakhshwan, X. Han, D.J. Gennardo, H.K. Pappas, H. Ju, Thin Solid Films 520 (2012) 5616–5626.
[25] A.J. Popel, A.M. Adamska, P.G. Martin, O.D. Payton, G.I. Lampronti, L. Picco, L. Payne, R. Springell, T.B. Scott, I. Monnet, C. Grygiel, I. Farnan, Nucl. Instr. Meth. Phys. Res. B. 386 (2016) 8–15.